

**Capabilities for  
a geostationary  
satellite to measure  
CO and O<sub>3</sub>**

M. Claeysman et al.

Title Page

Abstract

Introduction

Conclusions

References

Tables

Figures

⏪

⏩

◀

▶

Back

Close

Full Screen / Esc

Printer-friendly Version

Interactive Discussion



# A geostationary thermal infrared sensor to monitor the lowermost troposphere: O<sub>3</sub> and CO retrieval studies

M. Claeysman<sup>1,2</sup>, J.-L. Attié<sup>1,2</sup>, V.-H. Peuch<sup>2</sup>, L. El Amraoui<sup>2</sup>, W. A. Lahoz<sup>2,3</sup>,  
B. Josse<sup>2</sup>, P. Ricaud<sup>1</sup>, T. von Clarmann<sup>4</sup>, M. Höpfner<sup>4</sup>, J. Orphal<sup>4</sup>, J.-M. Flaud<sup>5</sup>,  
D. P. Edwards<sup>6</sup>, K. Chance<sup>7</sup>, X. Liu<sup>7</sup>, F. Pasternak<sup>8</sup>, and R. Cantié<sup>8</sup>

<sup>1</sup>Laboratoire d'Aérodologie, Université de Toulouse, CNRS/INSU, Toulouse, France

<sup>2</sup>CNRM-GAME, Météo-France and CNRS URA 1357, Toulouse, France

<sup>3</sup>NILU, N-2027 Kjeller, Norway

<sup>4</sup>Karlsruhe Institute of Technology, IMK, Karlsruhe, Germany

<sup>5</sup>Laboratoire Interuniversitaire des Systèmes Atmosphériques, CNRS UMR 7583,  
Université de Paris-Est, Créteil, France

<sup>6</sup>National Center for Atmospheric Research, Boulder, Colorado, USA

---

**Capabilities for  
a geostationary  
satellite to measure  
CO and O<sub>3</sub>**M. Claeysman et al.

---

[Title Page](#)[Abstract](#)[Introduction](#)[Conclusions](#)[References](#)[Tables](#)[Figures](#)[Back](#)[Close](#)[Full Screen / Esc](#)[Printer-friendly Version](#)[Interactive Discussion](#)

<sup>7</sup> Harvard-Smithsonian Center for Astrophysics, Cambridge, MA 02138, USA

<sup>8</sup> Astrium-EADS, Toulouse, France

Received: 26 July 2010 – Accepted: 27 July 2010 – Published: 18 August 2010

Correspondence to: M. Claeysman (marine.claeyman@aero.obs-mip.fr)

Published by Copernicus Publications on behalf of the European Geosciences Union.

## Abstract

This paper describes the capabilities of a nadir thermal infrared (TIR) sensor proposed for embarkation onboard a geostationary platform to monitor ozone (O<sub>3</sub>) and carbon monoxide (CO) for air quality (AQ) purposes. To assess the capabilities of this sensor we perform idealized retrieval studies considering typical atmospheric profiles of O<sub>3</sub> and CO over Europe with different instrument configurations (signal to noise ratio and spectral sampling interval) using the KOPRA forward model and the KOPRA-fit retrieval scheme based on the Tikhonov-Phillips regularization. We then select a configuration, referred to as GEO-TIR, optimized for providing information in the lowermost troposphere (LmT; 0–3 km in height). For the GEO-TIR configuration we obtain around 1.5 degrees of freedom for O<sub>3</sub> and 2 for CO at altitudes between 0 and 15 km. The error budget of GEO-TIR, calculated taking account of the principal contributions to the error (namely, temperature, measurement error, smoothing error) shows that information in the LmT can be achieved by GEO-TIR. We also retrieve analogous profiles from another geostationary infrared instrument with characteristics similar to the Meteosat Third Generation Infrared Sounder (MTG-IRS) which is dedicated to numerical weather prediction, referred to as GEO-TIR2. Comparison between GEO-TIR and GEO-TIR2 allows us to quantify the added value of GEO-TIR, a mission complementing the AQ observing system. To better characterize the information provided by GEO-TIR and GEO-TIR2 in the LmT, we retrieve two typical profiles of O<sub>3</sub> and CO for different thermal contrast ranging from –10 K to 10 K. The shape of the first averaging kernel (corresponding to the surface level) confirms that GEO-TIR has good sensitivity to CO in the LmT and also to O<sub>3</sub> for high positive thermal contrast. GEO-TIR2 has very low sensitivity in the LmT to O<sub>3</sub> but can have sensitivity to CO with high positive thermal contrast. To quantify these results for a realistic atmosphere, we simulate it using the chemical transport model MOCAGE (MOdèle de Chimie Atmosphérique à Grande Echelle) – this is the nature run. We simulate the O<sub>3</sub> and CO spatial and temporal distributions from GEO-TIR observations in the LmT in July 2009 over Europe by sampling the

### Capabilities for a geostationary satellite to measure CO and O<sub>3</sub>

M. Claeysman et al.

Title Page

Abstract

Introduction

Conclusions

References

Tables

Figures

⏪

⏩

◀

▶

Back

Close

Full Screen / Esc

Printer-friendly Version

Interactive Discussion



## Capabilities for a geostationary satellite to measure CO and O<sub>3</sub>

M. Claeysman et al.

Title Page

Abstract

Introduction

Conclusions

References

Tables

Figures

⏪

⏩

◀

▶

Back

Close

Full Screen / Esc

Printer-friendly Version

Interactive Discussion



nature run. Results show that GEO-TIR is able to capture well the spatial and temporal variability in the LmT for both O<sub>3</sub> and CO, particularly during periods with high positive thermal contrast near the ground and high surface temperature, which results in active photochemistry and a raised planetary boundary layer. These results also provide evidence of the significant added value in the LmT of GEO-TIR compared to GEO-TIR2 by showing GEO-TIR is closer to the nature run than GEO-TIR2 for various statistical parameters (correlation, bias, standard deviation).

### 1 Introduction

Air quality (AQ) is associated with the near surface atmospheric composition of trace gases and particles (Menut and Bessagnet, 2010). AQ is quantified using standards of concentration and deposition levels based on scientific knowledge of the impact of these pollutants on human health and the environment. Among species targeted by European policies, some are of greater concern as they more frequently exceed regulatory thresholds and require the public to be informed if this happens, examples include ground-level ozone (O<sub>3</sub>), nitrogen oxides (NO<sub>x</sub>) and suspended particulate matter (PM). Emissions of atmospheric pollutants from human activities are monitored and regulated at the European level by directives focusing both on activity sectors and national ceilings. Monitoring estimated and declared emissions is a challenge, owing to the complexity and number of emission sources. Among these, combustion sources (traffic, industry, residential use) are major contributors and need to be better simulated by models (e.g., Cuvelier et al., 2007; Vautard et al., 2007). Carbon monoxide (CO), an O<sub>3</sub> precursor, is a good tracer for combustion processes, including wild fires (e.g., Turquety et al., 2009). O<sub>3</sub> is an irritant which can affect severely the respiratory tract, in particular for people suffering from respiratory diseases, children and the elderly.

In the troposphere, the variability of sinks (including chemical losses such as from deposition), source strengths and transport and mixing processes, induces significant short term variations (one hour or less) of reactive species concentration (e.g., NO<sub>x</sub>). Relevant temporal (1 h) and spatial sampling scales (10 km×10 km) for observations



**Capabilities for a geostationary satellite to measure CO and O<sub>3</sub>**

M. Claeyman et al.

Title Page

Abstract

Introduction

Conclusions

References

Tables

Figures

◀

▶

◀

▶

Back

Close

Full Screen / Esc

Printer-friendly Version

Interactive Discussion



must be made at temporal resolutions appropriate for capturing the diurnal cycle (and shorter temporal time scales) in pollutants, and at spatial resolutions appropriate for capturing emissions and transcontinental transport of pollutants, or proxies for pollutants. The only observing platform that can provide this information is a geostationary (GEO) platform (Bovensmann and Orphal, 2005; Edwards, 2006). A GEO platform has the following desirable features: large scale observations that capture continental-scale emissions and processes (e.g., transport); repetitive observations to allow identification of temporal patterns and the production of long-term time-series; near simultaneous observations of key atmospheric composition variables; high temporal resolution observations to identify the temporal variability relevant to human society (e.g., diurnal and shorter time scales); and near-real-time observations for operational needs, as in Numerical Weather Prediction (NWP) and AQ forecasting.

Several GEO missions have been proposed for AQ in Europe, such as, GeoTropé (Burrows et al., 2004), and GeoFIS (Flaud et al., 2004; Orphal et al., 2005). In the USA, the GEO-CAPE mission (Edwards et al., 2009; National Research Council, 2007) is being recommended for launch in the 2013–2016 timeframe. In Japan, a similar mission has been proposed by the Japan Society of Atmospheric Chemistry to monitor O<sub>3</sub> from GEO (Akimoto et al. (2008); <http://www.stelab.nagoya-u.ac.jp/ste-www1/div1/taikiken/eisei/eisei2.pdf>, Japanese version only). In Europe, the Sentinel-4 payload (European Space Agency (ESA), 2007) will be embarked on the two Meteosat Third Generation Sounder (MTG-S) satellites in geostationary orbit, planned for launch in 2017 and 2024, respectively. The Sentinel 4 UVN (ultraviolet-visible-near infrared) mission is expected to provide measurements of O<sub>3</sub> and NO<sub>2</sub> column and aerosol optical depth. In order to complement the measurements provided by the Sentinel 4 UVN, the mission Monitoring the Atmosphere from Geostationary orbit for European Air Quality (MAGEAQ) has been proposed as a candidate for the Earth Explorer Opportunity Mission EE-8 call of the European Space Agency (Peuch et al., 2009, 2010). MAGEAQ is a multispectral instrument (thermal infrared and visible) designed to provide measurements of O<sub>3</sub> and CO in the LmT.

**Capabilities for  
a geostationary  
satellite to measure  
CO and O<sub>3</sub>**

M. Claeysman et al.

[Title Page](#)[Abstract](#)[Introduction](#)[Conclusions](#)[References](#)[Tables](#)[Figures](#)[Back](#)[Close](#)[Full Screen / Esc](#)[Printer-friendly Version](#)[Interactive Discussion](#)

Current AQ forecasting systems make little direct use of satellite measurements of chemical species, except through the use of global time-dependent chemical boundary conditions from global assimilation and forecast systems like the one demonstrated in the GEMS/MACC project (Global and regional Earth-system Monitoring using Satellite and in-situ data/Monitoring Atmospheric Composition and Climate), (Hollingsworth et al., 2008), or in the context of assessing biases and trends in emissions inventories (e.g., Kopacz et al., 2010). AQ systems mostly rely on surface observations to provide analyses as is done by the French air quality forecasting and monitoring system, Prev'air (Honoré et al., 2008). Increased use of satellite observations (notably from GEO platforms) by AQ forecasting systems is expected to improve their performance, with benefit to society.

In this paper, we describe a thermal infrared (TIR) instrument proposed for embarkation onboard a GEO platform (called GEO-TIR), optimized for monitoring O<sub>3</sub> and CO in the LmT for AQ purposes. Tools used for modelling radiative transfer and performing the retrieval of atmospheric state variables from remote measurements are described in Sect. 2. Section 3 assesses the sensitivity of the proposed instrument to atmospheric state variables relevant to AQ, and provides estimates of retrieval errors. We assess the added value of a GEO instrument dedicated to monitoring the LmT (GEO-TIR) compared to an instrument measuring in the same bands but with characteristics primarily optimized for temperature and humidity (GEO-TIR2), with particular emphasis on the capability to monitor O<sub>3</sub> and CO in the LmT. Retrieval studies are performed for several typical European atmospheric composition profiles to characterize the instrument configuration, and over atmospheric composition profiles covering Europe during summer to provide assessment of the instrument capabilities for a realistic atmosphere simulated by a state-of-the-art Chemistry Transport Model (CTM). Section 4 summarizes results and presents conclusions.

## 2 Retrieval of O<sub>3</sub> and CO

### 2.1 The forward model

The forward model KOPRA (Karlsruhe Optimized and Precise Radiative transfer Algorithm) is used to simulate the spectra measured by the proposed GEO-TIR instrument. KOPRA (Stiller et al., 2002) is a fast line-by-line code especially developed for analysis of data measured by high resolution interferometers. KOPRA was originally developed for the retrieval of spectra from the MIPAS (Michelson Interferometer for Passive Atmospheric Sounding) instrument onboard ENVISAT (Fischer et al., 2008). Recently it has been applied to the analysis of spectra measured from IASI on METOP-A (Eremenko et al., 2008).

Parallel to the forward calculation, KOPRA determines analytically the derivatives of the spectrum with respect to atmospheric and instrument retrieval parameters, namely the Jacobians (Höpfner et al., 1998). The KOPRA spectroscopic parameters are from the MIPAS database (Flaud et al., 2003) for O<sub>3</sub> and HITRAN 2004 (Rothman et al., 2005) for other species. High resolution atmospheric radiance spectra have been generated for cloud-free and aerosol-free conditions. Continua for carbon dioxide (Cousin et al., 1985) and water vapour (Clough, 1995) are also included.

### 2.2 Retrieval scheme

By using the analytical derivatives of the spectral signal with respect to the atmospheric state, a retrieval code was built around KOPRA. The retrieval code supports the simultaneous analysis of multiple spectral microwindows and various retrieval schemes. For the present analysis, the Tikhonov-Phillips regularization is employed (Tikhonov, 1963; Phillips, 1962):

$$\mathbf{x}_{i+1} = \mathbf{x}_i + (\mathbf{K}_i^T \mathbf{S}_y^{-1} \mathbf{K}_i + \gamma \mathbf{L}^T \mathbf{L})^{-1} \left[ \mathbf{K}_i^T \mathbf{S}_y^{-1} (\mathbf{y} - \mathbf{F}(\mathbf{x}_i)) - \gamma \mathbf{L}^T \mathbf{L} (\mathbf{x}_i - \mathbf{x}_a) \right] \quad (1)$$

where  $i$  is the index on the iterations,  $\mathbf{x}$  is the vector of atmospheric state variables to be retrieved,  $\mathbf{x}_a$  is the a priori profile,  $\mathbf{y}$  is the vector of the measured spectral radiances,

## Capabilities for a geostationary satellite to measure CO and O<sub>3</sub>

M. Claeysman et al.

Title Page

Abstract

Introduction

Conclusions

References

Tables

Figures

◀

▶

◀

▶

Back

Close

Full Screen / Esc

Printer-friendly Version

Interactive Discussion



## Capabilities for a geostationary satellite to measure CO and O<sub>3</sub>

M. Claeysman et al.

Title Page

Abstract

Introduction

Conclusions

References

Tables

Figures

◀

▶

◀

▶

Back

Close

Full Screen / Esc

Printer-friendly Version

Interactive Discussion



$K$  is the matrix of the partial derivatives of spectral radiances with respect to the atmospheric state variables,  $S_y$  is the measurement error covariance matrix,  $F$  represents the nonlinear forward model KOPRA,  $\gamma$  is a scalar user-defined regularization parameter, and  $L$  is a first order finite differences matrix, the  $T$  superscript represents the transpose. As commonly done, the regularization parameter  $\gamma$  is chosen to be as small as possible and adjusted empirically to avoid oscillations in the vertical profiles. The retrieval is performed from 0 to 39 km with a vertical step of 1 km. The state vector used in the retrieval scheme is the natural logarithm of the volume mixing ratio (VMR) values.

### 2.3 Error budget

A linear approach is used to estimate the total error on the retrieved products. The resulting total error consists of the following: the measurement error, the model parameters error and the smoothing error (Rodgers, 2000).

The retrieval noise  $S_n$  is the mapping of the measurement noise  $S_y$  onto the retrieval. Its error covariance matrix is calculated as:

$$S_n = G_y S_y G_y^T \quad (2)$$

where  $G_y$  is the gain matrix defined as:

$$G_y = (K^T S_y K + \gamma L^T L)^{-1} K^T S_y^{-1}. \quad (3)$$

The model parameters error  $S_p$  represents the uncertainty of parameters used in the radiative transfer simulation. The error covariance matrix for this contribution is:

$$S_p = G_y K_b S_b K_b^T G_y^T \quad (4)$$

where  $S_b$  is the error covariance matrix representing uncertainty of the parameters  $b$ , for example interfering species or temperature.  $K_b$  represents the Jacobians with respect to these parameters.

The smoothing error represents the error due to the limited vertical resolution of the retrieval. The error covariance matrix of the smoothing error can be expressed as:

$$\mathbf{S}_s = (\mathbf{A} - \mathbf{I})\mathbf{S}_e(\mathbf{A} - \mathbf{I})^T \quad (5)$$

where  $\mathbf{I}$  is the identity matrix,  $\mathbf{S}_e$  is the error covariance matrix of an ensemble of states which describes the variability of the atmosphere.  $\mathbf{A}$  is the averaging kernels matrix (AVK) representing the sensitivity of the retrieval to the true state, calculated as:

$$\mathbf{A} = \mathbf{G}_y \mathbf{K} = \left( \mathbf{K}^T \mathbf{S}_y \mathbf{K} + \gamma \mathbf{L}^T \mathbf{L} \right)^{-1} \mathbf{K}^T \mathbf{S}_y^{-1} \mathbf{K}. \quad (6)$$

The total error covariance matrix is given by:

$$\mathbf{S}_x = \mathbf{S}_n + \mathbf{S}_p + \mathbf{S}_s. \quad (7)$$

The errors described and discussed in this study correspond to the square roots of the diagonal elements of the calculated covariance matrices. The error is assumed unbiased, and is simulated randomly using a normal distribution.

### 3 Infrared instrument capabilities for O<sub>3</sub> and CO

Remote sensing from space in the TIR band has shown its value in the study of atmospheric chemistry (Clerbaux et al., 2003, and references therein). Tropospheric observations from LEO platforms have already demonstrated the potential for detecting constituents relevant for AQ. For example, Clerbaux et al. (2008b) demonstrate that the CO pollution arising from large cities and urban areas can be distinguished from the background transported pollution using MOPITT thermal IR retrievals during daytime and at locations where the thermal contrast (temperature at surface minus air temperature near the surface) is significant. A study over the Indian subcontinent from Kar et al. (2008) also shows that MOPITT provides information on LmT CO in selected continental regions with strong thermal contrast and could be useful for pollution studies. Dufour et al. (2010) present the capability of IASI to probe seasonal and day-to-day

## Capabilities for a geostationary satellite to measure CO and O<sub>3</sub>

M. Claeysman et al.

Title Page

Abstract

Introduction

Conclusions

References

Tables

Figures

⏪

⏩

◀

▶

Back

Close

Full Screen / Esc

Printer-friendly Version

Interactive Discussion



variations of lower tropospheric ozone on the regional scales of highly populated areas. Kar et al. (2010) show the possibility of detecting an urban signature in the tropospheric column ozone data derived from TOMS (Total Ozone Mapping Spectrometer) and OMI satellite data.

5 However, the main caveat of LEO satellites is their daily revisit time which does not allow them to observe the diurnal variability of atmospheric constituents. As a consequence, the only practical approach to observe atmospheric composition from space with a revisit time appropriate to the time scale of pollutants ( $\sim 1$  h) is from a geostationary orbit (Edwards, 2006).

### 10 3.1 Optimum instrument characteristics onboard a geostationary platform

Currently, six LEO instruments provide CO and/or O<sub>3</sub> observations from the IR thermal band; four from a nadir viewing platform: MOPITT (Drummond and Mand, 1996a) launched in 1999, AIRS (Aumann et al., 2003) launched in 2002, TES (Beer, 2006) launched in 2004 and IASI (Clerbaux et al., 2009) launched in 2006 and 2 from a limb-viewing platform: MIPAS (Michelson Interferometer for Passive Atmospheric Sounding) (Fischer et al., 2008) launched in 2002 and ACE (Atmospheric Chemistry Experiment) (Bernath et al., 2005) launched in 2003. All these instruments are based upon Fourier Transform Spectrometers (FTS), except MOPITT and AIRS which are a gas correlation radiometer and a grating spectrometer, respectively. The spectral sampling interval (SSI) of the FTS instruments varies from  $0.02 \text{ cm}^{-1}$  for ACE to  $0.25 \text{ cm}^{-1}$  for IASI. Recently, a study has been done to monitor pollution in the lower troposphere from a drifting orbit with a Static Infrared Fourier Transform Interferometer (SIFTI), (Pierangelo et al., 2008). SIFTI is defined with a SSI of  $0.0625 \text{ cm}^{-1}$  and a Noise Equivalent Spectral Radiance (NESR) of  $9.7 \text{ nW}/(\text{cm}^2 \text{ sr cm}^{-1})$  in the O<sub>3</sub> spectral band and  $0.91 \text{ nW}/(\text{cm}^2 \text{ sr cm}^{-1})$  in the CO spectral band.

25 In this study, we define an “optimum” instrument in the TIR band with a SSI and a Signal to Noise Ratio (SNR) chosen to obtain a maximum degree of freedom (DOF) in the troposphere (0–15 km). The DOF is calculated as the trace of the AVK (Rodgers,

## Capabilities for a geostationary satellite to measure CO and O<sub>3</sub>

M. Claeysman et al.

Title Page

Abstract

Introduction

Conclusions

References

Tables

Figures

⏪

⏩

◀

▶

Back

Close

Full Screen / Esc

Printer-friendly Version

Interactive Discussion





(Fig. 2), the DOFs vary from 0.35 to 2.15 for O<sub>3</sub> and from 0.9 to 3.5 for CO.

For AQ purposes, the main interest is to have a maximum of information in the LmT, documenting residual layers that are capable of mixing with the planetary boundary layer (PBL). Considering current IR instruments, technical feasibility and cost (Astrium-EADS, personal communication) a DOF of ~1.5 for O<sub>3</sub> and of ~2 for CO seems to be a good compromise to have vertical information in the troposphere. Figures 1 and 2 present the DOF according to the SNR and resolution. Considering characteristic values of DOFs providing information on O<sub>3</sub> and CO in the LmT (DOF=1.5 and 2, respectively), several pairs of (SNR, SSI) depending on the instrument concept (e.g. FTS, grating spectrometer), can be envisaged. In this idealized study, we select one configuration compatible for a FTS instrument (Table 1). However, for the same DOF but different (SNR, SSI) pairs, the retrieval results will not be very different (Figs. 1 and 2). For this reason, the results hereinafter presented with the chosen (SNR, SSI) pair do not depend on the instrument concept; they only depend on the SNR and SSI. For these specific configurations, the spectral microwindows have been selected according to a previous study on IASI (Clerbaux et al., 1998; Turquety et al., 2004) to avoid contamination by other species. The smoothing error, the measurement error and the temperature error are considered for these specific configurations. The contributions of the surface properties (surface temperature and emissivity) are not taken into account since they are low (e.g., Clerbaux et al., 2008a; Boynard et al., 2009) compared to other components (e.g., smoothing error). Note that the configuration selected is similar to the one chosen for the TIR sensor of MAGEAQ (Peuch et al., 2010).

Figure 3a and b presents the AVKs for O<sub>3</sub> for a positive thermal contrast (2K) corresponding to a SNR=750 and a SSI=0.05 cm<sup>-1</sup> and its corresponding error budget, respectively. The AVKs are calculated from 0 to 39 km with 1 km of vertical resolution but plotted from 0 to 20 km to focus on the troposphere and lower stratosphere. The lowermost maximum of the AVKs is located at 5 km, above the PBL which is situated at 1–2 km at noon in summer. The DOF obtained for heights below 15 km is 1.5. Figure 3b presents the different main components of the total error: measurement, temperature,

**Capabilities for a geostationary satellite to measure CO and O<sub>3</sub>**

M. Claeyman et al.

Title Page

Abstract

Introduction

Conclusions

References

Tables

Figures

⏪

⏩

◀

▶

Back

Close

Full Screen / Esc

Printer-friendly Version

Interactive Discussion



## Capabilities for a geostationary satellite to measure CO and O<sub>3</sub>

M. Claeyman et al.

Title Page

Abstract

Introduction

Conclusions

References

Tables

Figures

⏪

⏩

◀

▶

Back

Close

Full Screen / Esc

Printer-friendly Version

Interactive Discussion



smoothing and a priori errors. Given current absolute uncertainty in temperature observations, which is around 1 K for IASI (Pougetchev et al., 2009), an improvement up to a total uncertainty of 0.5 K will likely be achieved by combining the next generation satellite products like MTG-IRS and contemporary meteorological analyses systems.

Thus, we considered a temperature uncertainty of 0.5 K at each vertical level. Such an assumption was made in Clerbaux et al. (2008a). The temperature and measurement errors on the retrieved profile are low (less than 5%). The most important error is the smoothing error which is superimposed with the total error in Fig. 3b. At the surface, the total error (50%) is slightly lower than the a priori error (57%). In the same way, at altitudes of 2 and 3 km, namely at the top of the PBL or just above, the total error is lower than the a priori error: 15% instead of 30%, and 12% instead of 25%, respectively.

Figure 4a and b presents the same results but for CO with  $SSI=0.05\text{ cm}^{-1}$  and  $SNR=190$ . The lower maximum of the AVK is located at 3 km and the DOF obtained for heights below 15 km is  $\sim 2$ . The temperature error is larger than for O<sub>3</sub> and can reach 5% at the surface. The measurement error (around 2%) is still low compared to other error components. At the surface, at 2 km and 3 km in altitude the total error is always lower than the a priori error: 20%, 8% and 6% instead of 25% 11% and 10%, respectively.

As for AQ purposes we are interested in monitoring the LmT (0–3 km), we plot in Fig. 5 the surface AVKs for CO and O<sub>3</sub> as a function of the thermal contrast from –10 K to 10 K to better characterize the sensitivity of GEO-TIR in the LmT. We also simulate AVKs from another TIR instrument from a GEO platform with a configuration similar to that of Meteosat Third Generation InfraRed Sounder (MTG-IRS) (Stuhlmann et al., 2005), referred to as GEO-TIR2. It has a  $SSI$  of  $0.625\text{ cm}^{-1}$  for both O<sub>3</sub> and CO, and a noise of  $6.12\text{ nW}/(\text{cm}^2\text{ sr cm}^{-1})$  and  $24.5\text{ nW}/(\text{cm}^2\text{ sr cm}^{-1})$  for the CO and O<sub>3</sub> spectral windows, respectively (Clerbaux et al., 2008a). These noise values correspond to an SNR of 30 and 185 for CO and O<sub>3</sub>, respectively for a surface temperature of 280 K (Table 1). We simulate the observations from an instrument configuration close to

## Capabilities for a geostationary satellite to measure CO and O<sub>3</sub>

M. Claeysman et al.

Title Page

Abstract

Introduction

Conclusions

References

Tables

Figures

⏪

⏩

◀

▶

Back

Close

Full Screen / Esc

Printer-friendly Version

Interactive Discussion



MTG-IRS, which is dedicated to NWP (temperature and humidity), referred as GEO-TIR2, to determine the added value of GEO-TIR. MTG-IRS will be launched in the 2017–2018 timeframe and will measure radiances in the O<sub>3</sub> and CO TIR band but with an instrument configuration not optimized for AQ purposes. Figure 5 confirms the high dependence of the AVKs on the thermal contrast both for CO and O<sub>3</sub> for both GEO-TIR and GEO-TIR2. For CO with high positive thermal contrast (10 K), GEO-TIR can be sensitive at 1 km whereas for negative thermal contrast it is sensitive at 5 km and above. GEO-TIR2 is also sensitive in the LmT for CO for high positive thermal contrast, but the AVK values are low (AVKs<0.1) compared to GEO-TIR, for which values can reach 0.23. Concerning O<sub>3</sub>, GEO-TIR is less sensitive than for CO in the LmT. However, with high positive thermal contrast AVKs for O<sub>3</sub> can reach 0.15 at 3 km in altitude. GEO-TIR2 presents very low sensitivity in the LmT (AVKs<0.04) even with high positive thermal contrast. For both CO and O<sub>3</sub>, Fig. 5 shows that the GEO-TIR2 AVKs are broader than GEO-TIR ones, especially in the LmT, which confirms that GEO-TIR has a better vertical resolution.

These results show that a nadir instrument with the characteristics described in this section (GEO-TIR) can add information on O<sub>3</sub> and CO concentrations in the LmT compared to an instrument not optimized for AQ (GEO-TIR2). However, both instruments have generally low sensitivity to the surface. We note that the surface is already well covered by observations from European AQ networks (Honoré et al., 2008).

### 3.2 Geostationary observation system

To go a step further in our analysis, we simulate CO and O<sub>3</sub> retrieved profiles over Europe during summer, to better characterize the added value of a TIR instrument to monitor the LmT for a realistic atmosphere and not only for typical profiles as was done in Sect. 3.1. To study this added value, we first simulate the CO and O<sub>3</sub> observations from both platforms by sampling the atmosphere using the MOCAGE model (Peuch et al., 1999), a state-of-the-art three-dimensional CTM from Météo-France. MOCAGE simulates interactions between dynamical, physical and chemical processes in the

## Capabilities for a geostationary satellite to measure CO and O<sub>3</sub>

M. Claeyman et al.

Title Page

Abstract

Introduction

Conclusions

References

Tables

Figures

⏪

⏩

◀

▶

Back

Close

Full Screen / Esc

Printer-friendly Version

Interactive Discussion



troposphere and in the stratosphere. Its vertical resolution is 47 hybrid levels from the surface up to 5 hPa with a resolution of about 150 m in the LmT increasing to 800 m in the upper troposphere. MOCAGE is used for several applications: chemical weather forecasting at Météo-France (Dufour et al., 2004) and data assimilation research (e.g., El Amraoui et al., 2008, 2010). MOCAGE is also used in the operational AQ monitoring system in France: Prev'air (Rouïl et al., 2008) and in the pre-operational GMES atmosphere core service (Hollingsworth et al., 2008). The MOCAGE run which we sample is termed the nature run. We considered an error on the temperature profile of 0.5 K for both instruments (GEO-TIR and GEO-TIR2).

After sampling the atmosphere using MOCAGE (see above), the forward model KOPRA is used to generate corresponding atmospheric radiances seen by GEO-TIR and GEO-TIR2; these include representative values of SSI and noise on the signal. After producing these radiances, the KOPRA-fit retrieval scheme is used to produce CO and O<sub>3</sub> profiles for GEO-TIR and GEO-TIR2. To account for cloudy scenes, cloud estimates from the ARPEGE meteorological analysis (Courtier et al., 1991) are used to assign cloud fraction to the observation pixels. Pixels with a cloud fraction greater than 0.5 are filtered out, accounting for cloud coverage over Europe. Taken together, the different steps used to produce these CO and O<sub>3</sub> observations (see above) are termed the geostationary observation system (GOS).

Considering the high computational burden of such simulations, we select a day in summer, namely 12 July 2009, representative of a typical northern summer day, with no meteorological or pollution major event, to simulate observations from both satellites over Europe. The meteorological situation for 12 July 2009, shows an anticyclone over the Mediterranean sea and a low-pressure area over the North West of Ireland which generates a westerly wind flow over Western Europe. That day was cloudy over Northern Europe and clear over the Mediterranean Basin which leads to a European-wide cloud cover of 50%, which is represented in Fig. 6 by the grey area. Figure 6 represents the surface temperature and the thermal contrast at 00:00 UTC and at 12:00 UTC on 12 July 2009 from the ARPEGE model. During night, low surface

temperature and negative thermal contrast are observed over land (the latter can reach  $-8$  K over France), whereas during daytime high surface temperature and positive thermal contrast are observed (the latter can reach  $15$  K over Spain or North Africa). Over sea the thermal contrast is close to  $0$  K or slightly positive. The thermal contrast and surface temperature are important factors to take into account for observations in the TIR spectral region. Deeter et al. (2007) showed that with high positive thermal contrast and high surface temperature, nadir TIR instruments are more sensitive to information in the LmT.

### 3.3 Comparison of geostationary thermal infrared observations of $O_3$ and CO

#### 3.3.1 Spatial distributions of retrieved $O_3$ and CO

Figure 7 presents  $O_3$  concentrations at  $3$  km on 12 July 2009 during nighttime (00:00 UTC) and daytime (12:00 UTC) simulated by MOCAGE (the nature run), and simulated by the GOS for GEO-TIR and GEO-TIR2. The grey area corresponds to pixels with more than 50% cloud-fraction, where retrievals are not done. MOCAGE CO and  $O_3$  fields have not been smoothed by GEO-TIR and GEO-TIR2 AVKs in order to represent the total error (see Sect. 2.3) in the comparison with both satellites. In the nature run (Fig. 7c and f) maxima of  $O_3$  are observed over the Atlantic Ocean and France and are moving from West to East. The main spatial patterns of  $O_3$  are represented well by GEO-TIR (Fig. 7a and d) with a minimum of  $O_3$  concentrations over North West Spain, North Africa and North East Iceland. The maxima are also well represented over Spain and over the Mediterranean Sea. However, Fig. 7g and i shows that the differences (total error) between the nature run and GEO-TIR range between  $-40\%$  (over land) and  $70\%$  (over sea). Globally, GEO-TIR  $O_3$  concentrations are smooth compared to the nature run: GEO-TIR minima are higher in magnitude than the nature run ones and GEO-TIR maxima are lower in magnitude than the nature run ones. Over France during nighttime, GEO-TIR does not capture the maxima of the  $O_3$  concentrations, whereas during daytime, it captures well the maxima over

## Capabilities for a geostationary satellite to measure CO and $O_3$

M. Claeysman et al.

Title Page

Abstract

Introduction

Conclusions

References

Tables

Figures

◀

▶

◀

▶

Back

Close

Full Screen / Esc

Printer-friendly Version

Interactive Discussion



**Capabilities for  
a geostationary  
satellite to measure  
CO and O<sub>3</sub>**

M. Claeyman et al.

Title Page	
Abstract	Introduction
Conclusions	References
Tables	Figures
⏪	⏩
◀	▶
Back	Close
Full Screen / Esc	
Printer-friendly Version	
Interactive Discussion	

Spain. Figure 7b, e, h and j, representing the O<sub>3</sub> concentrations from GEO-TIR2 and the relative differences from the nature run, show a latitudinal gradient which suggests that GEO-TIR2 is more sensitive to the upper layers of the atmosphere, where the latitudinal gradient of O<sub>3</sub> is strong and is contaminated by the a priori information in the LmT.

Figure 8a and b represents the DOFs between 0 and 15 km obtained for GEO-TIR for O<sub>3</sub> over the same period studied previously, 12 July 2009. The DOFs are between 1.1 and 1.8 depending on the thermal contrast and surface temperature (Fig. 6). Over the land, during daytime and with a high positive thermal contrast and high surface temperature, the DOFs are high (~1.8) whereas during nighttime, with a negative thermal contrast and low surface temperature, they are low (~1.1). Over the sea, where the thermal contrast is less sensitive to the diurnal variation (Fig. 6), the DOFs are about 1.5 both during daytime and nighttime. Figure 8c and d represents the DOFs for GEO-TIR2. Similar remarks as for GEO-TIR can be made regarding the evolution of the DOFs with the thermal contrast and the surface temperature but the values are between 0.5 and 0.85. Figure 8e,f and g,h, represents the peak altitude of the lowermost AVKs of the retrieved O<sub>3</sub> from GEO-TIR and GEO-TIR2, respectively. This diagnostic is used to determine the sensitivity of the instrument to the LmT. Over land, GEO-TIR is sensitive for O<sub>3</sub> around 2 km during daytime and at 4 km during nighttime whereas GEO-TIR2 is sensitive for O<sub>3</sub> at 14 km during daytime and at 16 km during nighttime. Over sea, the lowermost maximum of the AVKs from GEO-TIR is between 2 and 7 km and for GEO-TIR2 is between 14 and 17 km. Figure 8g and h confirms that GEO-TIR2 is mainly sensitive for O<sub>3</sub> to the upper troposphere and lower stratosphere, which is in agreement with the latitudinal gradient of O<sub>3</sub> concentrations observed in Fig. 7e,f and results found in Sect. 3.1. The difference between GEO-TIR2 and the nature run can reach 140% (e.g., over the Atlantic ocean).

Figure 9 presents CO concentrations at 3 km on 12 July 2009 during nighttime (00:00 UTC) and daytime (12:00 UTC) simulated by the nature run and simulated with the GOS for GEO-TIR and GEO-TIR2. In the nature run (Fig. 9c and f), maxima of



---

**Capabilities for  
a geostationary  
satellite to measure  
CO and O<sub>3</sub>**M. Claeyman et al.

---

[Title Page](#)[Abstract](#)[Introduction](#)[Conclusions](#)[References](#)[Tables](#)[Figures](#)[⏪](#)[⏩](#)[◀](#)[▶](#)[Back](#)[Close](#)[Full Screen / Esc](#)[Printer-friendly Version](#)[Interactive Discussion](#)

CO are observed over the Atlantic Ocean, Western Spain and Italy and minima are observed over the Atlantic Ocean. Figure 9a and b shows that CO observations from GEO-TIR are close to the nature run (Fig. 9c and f). They present maxima over North West Spain, in the Mediterranean Sea near Sardinia and Sicily and over Italy. The minima are also well represented over North East Iceland, over South West Spain and over the South East Mediterranean Basin. Figure 9g and i shows that the differences between GEO-TIR and the nature run are between  $-25\%$  and  $30\%$  for CO and are lower in magnitude than for O<sub>3</sub>. However, GEO-TIR CO concentrations are smoother compared to the nature run ones (GEO-TIR minima in magnitude are higher than the nature run ones and GEO-TIR maxima in magnitude are lower than the nature run ones). Figure 9b,e,h and j presents similar results for GEO-TIR2. In opposition to the GEO-TIR2 O<sub>3</sub> results, GEO-TIR2 is able to capture some CO horizontal spatial patterns over North East Iceland and over North West Spain. However, the maxima of CO concentrations in GEO-TIR2 observations over the South East Mediterranean Basin are not comparable in magnitude with those of the MOCAGE nature run at 3 km of altitude. Similar maxima are observed in the nature run around 11 km (not shown) which may indicate that GEO-TIR2 observations of CO at 3 km can be affected by higher CO concentrations at higher levels in altitude. The differences between GEO-TIR2 and the nature run for CO are between  $-30\%$  and  $70\%$ .

Figure 10a and b shows that the DOFs for CO between 0 and 15 km obtained for GEO-TIR are between 1.5 (over sea) and 2.5 (over land during daytime) and Fig. 10c and d indicates that the DOFs obtained for GEO-TIR2 CO are close to 1. Figure 10e and f shows that GEO-TIR is sensitive for CO at 1 km during daytime over land and between 3 and 4 km over sea and during nighttime. Figure 10g and h shows that GEO-TIR2 is sensitive for CO at the altitude of 1 km over particular locations where there is very high positive thermal contrast. However, it is generally sensitive between 5 and 6 km of altitude. A DOF of 1 means that GEO-TIR2 can monitor the tropospheric CO column as presented by Clerbaux et al. (2004, 2008a). CO maxima can be detected when they are located in the lower troposphere with high positive thermal contrast,



## Capabilities for a geostationary satellite to measure CO and O<sub>3</sub>

M. Claeyman et al.

Title Page

Abstract

Introduction

Conclusions

References

Tables

Figures

⏪

⏩

◀

▶

Back

Close

Full Screen / Esc

Printer-friendly Version

Interactive Discussion

indicates good monitoring capabilities for the GEO-TIR in the LmT. The bias between GEO-TIR and the nature run is mainly positive for the 0–3 and 0–6 km columns which reflects the overestimation of O<sub>3</sub> concentrations observed in Fig. 11. The standard deviation of the differences between GEO-TIR and the nature run is ~12% for the O<sub>3</sub> 0–3 km column and ~8% for the O<sub>3</sub> 0–6 km column. As opposed to GEO-TIR, Fig. 11 and Table 2 show that GEO-TIR2 has very low sensitivity to O<sub>3</sub> in the LmT.

As for O<sub>3</sub>, GEO-TIR represents well the diurnal variability, the maxima and the minima over all 6 cities for the CO 0–3 km column (Fig. 11). This indicates that even with low thermal contrast GEO-TIR is able to capture the variability of the CO 0–3 km column. The bias between GEO-TIR and the nature run is mainly negative (~6% for the CO 0–3 km column and ~4% for the CO 0–6 km column) over all the 6 cities since GEO-TIR captures the maxima of CO but with an under-estimation. This is because the maximum values of CO in the nature run are located in the layer near the surface (0–500 m) where GEO-TIR is less sensitive. The standard deviation is ~6% for the CO 0–3 km column and ~4% for the CO 0–6 km column. The correlation between the nature run and GEO-TIR is between 0.79 and 0.90 for the CO 0–3 km column and between 0.85 and 0.91 for the CO 0–6 km column. Figure 11 and Table 2 also show that GEO-TIR2 presents better results in the LmT for CO than for O<sub>3</sub> as explained previously in Sect. 3.3.1. The correlation between GEO-TIR2 and the nature run for the CO 0–3 km column, is between 0.39 and 0.74 and between 0.52 and 0.85 for the CO 0–6 km columns. Agreement between GEO-TIR and the nature run is better than that between GEO-TIR2 and the nature run, as evidenced by the higher correlations for the former comparison. This shows the capabilities of GEO-TIR to measure O<sub>3</sub> and CO in the LmT, and its added value with respect to GEO-TIR2.

## 4 Summary and conclusions

In this paper, we describe retrieval studies to evaluate the capability of a nadir TIR sensor with high SNR and SSI, onboard a geostationary platform, for monitoring O<sub>3</sub>

**Capabilities for a geostationary satellite to measure CO and O<sub>3</sub>**

M. Claeysman et al.

and CO in the lowermost troposphere (LmT; 0–3 km) over Europe. For simulated O<sub>3</sub> and CO profiles, we calculate the DOFs for different instrument configurations (SNR and SSI) for a positive (+2 K) and negative (–2 K) thermal contrast for an idealized case, considering all the parameters (e.g., regularization) fixed except the SSI and the SNR. We note that several instrument configurations can lead to the same DOF (a low SSI with a high SNR can be equivalent to a high SSI with a low SNR). From these results, we select a particular instrument configuration that is technically achievable (SSI=0.05 cm<sup>-1</sup> and SNR=750 for O<sub>3</sub>; SSI=0.5 cm<sup>-1</sup> and SNR=190 for CO), called GEO-TIR, and simulate the main error components (smoothing error, measurement error and temperature error). For O<sub>3</sub> and CO, we find that an instrument with these characteristics can provide information in the LmT. At an altitude of 2 km, the total error is lower than the a priori error: 15% instead of 30% for O<sub>3</sub> and 8% instead of 11% for CO.

MTG-IRS is a nadir TIR sensor which is planned to be onboard a geostationary platform, and will be dedicated to measure temperature and humidity. However, as MTG-IRS will be launched in the 2016–2018 timeframe and will measure radiances in the CO and O<sub>3</sub> TIR bands, we simulate an infrared geostationary instrument (GEO-TIR2) with characteristics similar to MTG-IRS to quantify the added value of a nadir TIR sensor complementing the air quality (AQ) observing system (GEO-TIR). To better characterize the information provided by GEO-TIR and GEO-TIR2 in the LmT, we retrieve two typical profiles of O<sub>3</sub> and CO for different thermal contrast, positive and negative. The shape of the first averaging kernel (corresponding to the surface level) confirms that GEO-TIR shows good sensitivity for CO in the LmT and for O<sub>3</sub> for high positive thermal contrast. However, GEO-TIR2 shows very low sensitivity in the LmT for O<sub>3</sub> but can be sensitive with high positive thermal contrast for CO. We confirm that the shape of the averaging kernels of TIR instruments is highly dependent on the thermal contrast.

O<sub>3</sub> and CO distributions over Europe as measured by GEO-TIR and the future GEO-TIR2 are simulated. This is done using results of the 3-D CTM MOCAGE coupled with

Title Page

Abstract

Introduction

Conclusions

References

Tables

Figures

⏪

⏩

◀

▶

Back

Close

Full Screen / Esc

Printer-friendly Version

Interactive Discussion



---

**Capabilities for  
a geostationary  
satellite to measure  
CO and O<sub>3</sub>**M. Claeyman et al.

---

[Title Page](#)[Abstract](#)[Introduction](#)[Conclusions](#)[References](#)[Tables](#)[Figures](#)[⏪](#)[⏩](#)[◀](#)[▶](#)[Back](#)[Close](#)[Full Screen / Esc](#)[Printer-friendly Version](#)[Interactive Discussion](#)

a radiative transfer model KOPRA and its associated retrieval scheme KOPRA-fit. The simulation of spatial variability during nighttime and daytime of GEO-TIR observations shows that GEO-TIR simulates well the horizontal O<sub>3</sub> and CO spatial patterns at 3 km compared to the nature run provided by MOCAGE. The maxima and minima in magnitude are generally well detected but smoother compared to those in the nature run. The DOFs calculated for 0–15 km are between 1.1 and 1.8 for O<sub>3</sub> and between 1.5 and 2.5 for CO, depending on the surface thermal contrast. Conversely, GEO-TIR2 shows very low sensitivity to the O<sub>3</sub> in the LmT and the concentrations at 3 km reflect the O<sub>3</sub> latitudinal gradient observed in the upper layers of the troposphere. The DOFs obtained for CO in the troposphere is around 1, which indicates that GEO-TIR2 is sensitive to the CO tropospheric column. In the case of high positive thermal contrast and high surface temperature, GEO-TIR2 has sensitivity to CO in the LmT. However, it is difficult to discriminate CO in the middle or upper troposphere and CO in the LmT, because GEO-TIR2 has just CO column information (DOF~1). Simulations of the temporal evolution of the 0–3 km column show that GEO-TIR is able to capture well the variability in O<sub>3</sub> and CO and the diurnal cycle with high positive thermal contrast and high surface temperature. The correlation between GEO-TIR and the nature run is between 0.71 and 0.81 for O<sub>3</sub> (0–3 km column) and between 0.79 and 0.90 for CO (0–3 km column). Concerning GEO-TIR2, it presents very low sensitivity to the O<sub>3</sub> concentration in the LmT and some sensitivity to CO concentrations with favourable conditions (e.g. high concentration in the LmT and high positive thermal contrast). The correlations between the nature run and GEO-TIR2 are lower than the GEO-TIR ones.

These results show that a nadir TIR sensor onboard a GEO platform with a specific instrument configuration (high SNR and SSI) is sensitive to the LmT especially for positive thermal contrast and high surface temperature (typically over land during daytime) for both CO and O<sub>3</sub>. We have shown that such a configuration (GEO-TIR) is capable of bringing added value in the LmT compared to a configuration optimized for numerical weather prediction (GEO-TIR2). In a subsequent study, we will make observing system simulation experiments (OSSEs) to further quantify the impact of such a satellite

instrument on AQ analyses and forecasts. Future work will also concern multispectral retrievals to improve these measurements at the surface, with a methodology similar to that of Worden et al. (2007) for TES and OMI concerning TIR and the ultraviolet spectral region. In particular, adding channels in the visible (Chappuis bands) as for the MAGEAQ instrument, should improve sensitivity to O<sub>3</sub> concentrations in the near surface, likely reaching between 2.5 and 3 DOFs for O<sub>3</sub> in the troposphere, and thus providing effective sounding capability for the LmT. For improving CO measurements at the surface, one possibility is to add a near infrared band as was done by Edwards et al. (2009) and proposed in GEO-CAPE. Regarding the relevance of the added value of GEO-TIR, such a mission could be a key part of future plans for the Global Observing System.

*Acknowledgements.* This work was funded by the Centre National de Recherches Scientifiques (CNRS), Astrium-EADS, the Centre National de Recherches Météorologiques (CNRM) of Météo-France and the RTRA/STAE (project POGEQA). The authors acknowledge ETHER, the French atmospheric composition database (CNES and CNRS-INSU) and the Région Midi-Pyrénées (project INFOAIR).



The publication of this article is financed by CNRS-INSU.

## AMTD

3, 3489–3534, 2010

### Capabilities for a geostationary satellite to measure CO and O<sub>3</sub>

M. Claeysman et al.

Title Page

Abstract

Introduction

Conclusions

References

Tables

Figures

⏪

⏩

◀

▶

Back

Close

Full Screen / Esc

Printer-friendly Version

Interactive Discussion



## References

- Akimoto, H., Irie, H., Kasai, Y., Kanaya, Y., Kita, K., Koike, M., Kondo, Y., Nakazawa, T., and Hayashida, S.: Planning a geostationary atmospheric observation satellite, Commission on the Atmospheric Observation Satellite of the Japan Society of Atmospheric Chemistry, 2008. 3494
- Aumann, J. H., Chahine, M. T., Gautier, C., Goldberg, M. D., McMillin, E. K. L. M., Revercomb, H., Rosenkranz, P. W., Smith, W. L., Staelin, D. H., Strow, L. L., and Susskind, J.: AIRS/AMSU/HSB on the Aqua Mission: Design, Science Objectives, Data Products, and Processing Systems, *IEEE T. Geosci. Remote*, 41, 253–264, 2003. 3499
- Beer, R.: TES on the aura mission: scientific objectives, measurements, and analysis overview, *IEEE T. Geosci. Remote*, 44, 1102–1105, 2006. 3499
- Beer, R., Glavich, T. A., and Rider, D. M.: Tropospheric emission spectrometer for the earth observing system's Aura satellite, *Appl. Optics*, 40, 2356–2367, 2001. 3493
- Bernath, P. F., McElroy, C. T., Abrams, M. C., Boone, C. D., Butler, M., Camy-Peyret, C., Carleer, M., Clerbaux, C., Coheur, P. F., Colin, R., DeCola, P., DeMazière, M., Drummond, J. R., Dufour, D., Evans, W. F. J., Fast, H., Fussen, D., Gilbert, K., Jennings, D. E., Llewellyn, E. J., Lowe, R. P., et al.: Atmospheric Chemistry Experiment (ACE): mission overview, *Geophys. Res. Lett.*, 32, L15S01, doi:10.1029/2005GL022386, 2005. 3499
- Bovensmann, H., Burrows, J.-P., Buchwitz, M., Frerick, J., Noel, S., Rozanov, V. V., Chance, K. V., and Goede, A. P. H.: SCIAMACHY: mission objectives and measurement modes, *J. Atmos. Sci.*, 56, 127–150, 1999. 3493
- Bovensmann, H. and Orphal, J.: The geostationary component of an operational atmospheric chemistry monitoring system: Specification and expected performance, *ESA Study: Operational Atmospheric Chemistry Monitoring Missions 17237/03/NL/GS (CAPACITY)*, 2005. 3494
- Boynard, A., Clerbaux, C., Coheur, P.-F., Hurtmans, D., Turquety, S., George, M., Hadji-Lazaro, J., Keim, C., and Meyer-Arneke, J.: Measurements of total and tropospheric ozone from IASI: comparison with correlative satellite, ground-based and ozonesonde observations, *Atmos. Chem. Phys.*, 9, 6255–6271, doi:10.5194/acp-9-6255-2009, 2009. 3501
- Burrows, J. P., Bovensmann, H., Bergametti, G., Flaud, J. M., Orphal, J., Noël, S., Monks, P. S., Corlett, G. K., Goede, A. P., von Clarmann, T., Steck, T., Fischer, H., and Friedl-Vallon, F.: The geostationary tropospheric pollution explorer (GeoTROPE) mission: objectives, require-

AMTD

3, 3489–3534, 2010

### Capabilities for a geostationary satellite to measure CO and O<sub>3</sub>

M. Claeysman et al.

Title Page

Abstract

Introduction

Conclusions

References

Tables

Figures

⏪

⏩

◀

▶

Back

Close

Full Screen / Esc

Printer-friendly Version

Interactive Discussion

## Capabilities for a geostationary satellite to measure CO and O<sub>3</sub>

M. Claeysman et al.

Title Page

Abstract

Introduction

Conclusions

References

Tables

Figures

◀

▶

◀

▶

Back

Close

Full Screen / Esc

Printer-friendly Version

Interactive Discussion



ments and mission concept, *Adv. Space Res.*, 34, 682–687, 2004. 3494

Burrows, J. P., Weber, M., Buchwitz, M., Rozanov, V., Ladstätter-Weissenmayer, A., Richter, A., DeBeek, R., Hoogen, R., Bramstedt, K., Eichmann, K. U., and Eisinger, M.: The global ozone monitoring experiment (GOME): Mission concept and first scientific results, *J. Atmos. Sci.*, 56, 151–175, 1999. 3493

Callies, J., Corpaccioli, E., Eisinger, M., Hahne, A., and Lefebvre, A.: GOME-2 Metops Second-Generation Sensor for Operational Ozone Monitoring, *Esa bull.*, No. 102, 28–36, 2000. 3493

Clerbaux, C., Boynard, A., Clarisse, L., George, M., Hadji-Lazaro, J., Herbin, H., Hurtmans, D., Pommier, M., Razavi, A., Turquety, S., Wespes, C., and Coheur, P.-F.: Monitoring of atmospheric composition using the thermal infrared IASI/MetOp sounder, *Atmos. Chem. Phys.*, 9, 6041–6054, doi:10.5194/acp-9-6041-2009, 2009. 3493, 3499, 3500

Clerbaux, C., Chazette, P., Hadji-Lazaro, J., Mégie, G., Müller, J.-F., and Clough, S. A.: Remote sensing of CO, CH<sub>4</sub>, and O<sub>3</sub> using a spaceborne nadir-viewing interferometer, *J. Geophys. Res.*, 103(D15), 18999–19013, 1998. 3501

Clerbaux, C., Coheur, P.-F., Hurtmans, D., Hadji-Lazaro, J., Turquety, S., and van Oss, R.: Capabilities of MTG-IRS to sound ozone, CO and methane using ESA pre-phase A specifications, *Eumetsat EUM/CO/05/1484/SAT*, 2004. 3507

Clerbaux, C., Coheur, P.-F., Turquety, S., and Hadji-Lazaro, J.: Capabilities of infrared sounder observations for monitoring atmospheric composition and chemistry applications, *Eumetsat EUM/CO/O3/1127/SAT*, 2003. 3498

Clerbaux, C., Coheur, P.-F., Scharf, O., Hurtmans, D., and Boynard, A.: The potential of MTG-IRS and S4-TIR to detect high pollution events at urban and regional scales, *Eumetsat EUM/CO/07/460000447/SAT*, 2008a. 3501, 3502, 3507

Clerbaux, C., Edwards, D. P., Deeter, M., Emmons, L., Lamarque, J.-F., Tie, X. X., Massie, S. T., and Gille, J.: Carbon monoxide pollution from cities and urban areas observed by the Terra/MOPITT mission, *Geophys. Res. Lett.*, 35, L03817, doi:10.1029/2007GL032300, 2008b. 3498

Clough, S. A.: The water vapor continuum and its role in remote sensing, *Atmospheric and Environmental Research, Inc., Optical Remote Sensing of the Atmosphere*, 22, 76–78, 1995. 3496

Courtier, P., Freydier, C., Geleyn, J. F., Rabier, F., and Rochas, M.: The ARPEGE project at Météo France, in: *Atmospheric Models, Vol. 2, Workshop on Numerical Methods*, Reading, UK, 193–231, 1991. 3504



## Capabilities for a geostationary satellite to measure CO and O<sub>3</sub>

M. Claeysman et al.

Title Page

Abstract

Introduction

Conclusions

References

Tables

Figures

◀

▶

◀

▶

Back

Close

Full Screen / Esc

Printer-friendly Version

Interactive Discussion

CO assimilated fields, *Atmos. Chem. Phys.*, 10, 2175–2194, doi:10.5194/acp-10-2175-2010, 2010. 3504

El Amraoui, L., Semane, N., Peuch, V.-H., and Santee, L.: Investigation of dynamical processes in the polar stratospheric vortex during the unusually cold winter 2004/2005, *Geophys. Res. Lett.*, 35, L03803, doi:10.1029/2007GL031251, 2008. 3504

Eremenko, M., Dufour, G., Foret, G., Keim, C., Orphal, J., Beekmann, M., Bergametti, G., and Flaud, J.-M.: Tropospheric ozone distributions over Europe during the heat wave in July 2007 observed from infrared nadir spectra recorded by IASI, *Geophys. Res. Lett.*, 35, L18805, doi:10.1029/2008GL03803, 2008. 3496, 3500

European Space Agency (ESA): GMES Sentinels 4 and 5 Mission Requirement Document, EOP-SMA/1507, 2007. 3494

Fischer, H., Birk, M., Blom, C., Carli, B., Carlotti, M., von Clarmann, T., Delbouille, L., Dudhia, A., Ehhalt, D., Endemann, M., Flaud, J. M., Gessner, R., Kleinert, A., Koopman, R., Langen, J., López-Puertas, M., Mosner, P., Nett, H., Oelhaf, H., Perron, G., Remedios, J., Ridolfi, M., Stiller, G., and Zander, R.: MIPAS: an instrument for atmospheric and climate research, *Atmos. Chem. Phys.*, 8, 2151–2188, doi:10.5194/acp-8-2151-2008, 2008. 3496, 3499

Flaud, J. M., Orphal, J., Bergametti, G., Deniel, C., von Clarmann, T., Friedl-Vallon, F., Steck, T., Fischer, H., Bovensmann, H., Burrows, J. P., Carlotti, M., Ridolfi, M., and Palchetti, L.: The Geostationary Fourier Imaging Spectrometer (GeoFIS) as part of the Geostationary Tropospheric Pollution Explorer (GeoTroPE) mission: objectives and capabilities, *Adv. Space Res.*, 34, 688–693, 2004. 3494

Flaud, J.-M., Piccolo, C., Carli, B., Perrin, A., Coudert, L. H., Teffo, J.-L., and Brown, L. R.: Molecular line parameters for the MIPAS (Michelson Interferometer for Passive Atmospheric Sounding) experiment, *Atmos. Oceanic Opt.*, 16, 172–182, 2003. 3496

Hollingsworth, A., Engelen, R., Textor, C., Boucher, O., Chevallier, F., Dethof, A., Elbern, H., Eskes, H., Flemming, J., Granier, C., Kaiser, J. W., Morcrette, J. J., Rayner, P., Peuch, V.-H., Rouïl, L., and the GEMS Consortium: Toward a monitoring and forecasting system for atmospheric composition: The GEMS Project, *B. Am. Meteor. Soc.*, 89(8), 1147–1164, 2008. 3495, 3504

Honoré, C., Rouïl, L., Vautard, R., Beekmann, M., Bessagne, B., Dufour, A., Elichegaray, C., Flaud, J.-M., Malherbe, L., Meleux, F., Menut, L., Martin, D., Peuch, A., Peuch, V.-H., and Poisson, N.: Predictability of European air quality: Assessment of 3 years of operational forecasts and analyses by the PREV’AIR system, *J. Geophys. Res.*, 113, D04301,

## Capabilities for a geostationary satellite to measure CO and O<sub>3</sub>

M. Claeysman et al.

Title Page

Abstract

Introduction

Conclusions

References

Tables

Figures

◀

▶

◀

▶

Back

Close

Full Screen / Esc

Printer-friendly Version

Interactive Discussion



doi:10.1029/2007JD008761, 2008. 3495, 3503

Höpfner, M., Stiller, G. P., Kuntz, M., von Clarmann, T., Echle, G., Funke, B., Glatthor, N., Hase, F., Kemnitzer, H., and Zorn, S.: The Karlsruhe optimized and precise radiative transfer algorithm. Part II: Interface to retrieval applications, in: *Optical Remote Sensing of the Atmosphere and Clouds*, Beijing, China, 15–17 September 1998, edited by: Wang, J., Wu, B., Ogawa, T., and Guan, Z., 3501, 186–195, 1998. 3496

Kar, J., Fishman, J., Creilson, J. K., Richter, A., Ziemke, J., and Chandra, S.: Are there urban signatures in the tropospheric ozone column products derived from satellite measurements?, *Atmos. Chem. Phys.*, 10, 5213–5222, doi:10.5194/acp-10-5213-2010, 2010. 3499

Kar, J., Jones, D. B. A., Drummond, J. R., Attie, J.-L., Liu, J., Zou, J., Nichitiu, F., Seymour, M. D., Edwards, D. P., Deeter, M. N., Gille, J. C., and Richter, A.: Measurement of low-altitude CO over the Indian subcontinent by MOPITT, *J. Geophys. Res.*, 113, D16307, doi:10.1029/2007JD009362, 2008. 3498

Kobayashi, H., Shimota, A., Kondo, K., Okumura, E., Kameda, Y., Shimoda, H., and Ogawa, T.: Development and evaluation of the interferometric monitor for greenhouse gases: a high-throughput Fourier-transform infrared radiometer for nadir Earth observation, *Appl. Optics*, 38, 6801–6807, 1999. 3493

Kopacz, M., Jacob, D. J., Fisher, J. A., Logan, J. A., Zhang, L., Megretskaia, I. A., Yantosca, R. M., Singh, K., Henze, D. K., Burrows, J. P., Buchwitz, M., Khlystova, I., McMillan, W. W., Gille, J. C., Edwards, D. P., Eldering, A., Thouret, V., and Nedelec, P.: Global estimates of CO sources with high resolution by adjoint inversion of multiple satellite datasets (MOPITT, AIRS, SCIAMACHY, TES), *Atmos. Chem. Phys.*, 10, 855–876, doi:10.5194/acp-10-855-2010, 2010. 3495

Levelt, P. F., van den Oord, G. H. J., Dobber, M. R., Mslkki, A., Visser, H., Vries, J., Stammes, P., Lundell, J. O. V., and Saari, H.: The Ozone monitoring instrument, *IEEE T. Geosci. Remote*, 44(5), 1093–1101, doi:0.1109/TGRS.2006.872333, 2006. 3493

Martin, R. V.: Satellite remote sensing of surface air quality, *Atmos. Environ.*, 42, 7823–7843, 2008. 3493

Menut, L. and Bessagnet, B.: Atmospheric composition forecasting in Europe, *Atmos. Environ.*, 28, 61–74, 2010. 3492

McMillan, W. W., Barnet, C., Strow, L., Chahine, M., McCourt, M., Novelli, P., Korontzi, S., Maddy, E., and Datta, S.: Daily global maps of carbon monoxide: first views from NASA's atmospheric infrared sounder, *Geophys. Res. Lett.*, 32, L11801, doi:10.1029/2004GL012,821,

2005. 3493

National Research Council: Earth Science and Applications from Space: National Imperatives for the Next Decade and Beyond, in: National Academy of Sciences, Washington, DC, USA, 2007. 3494

5 Orphal, J., Bergametti, G., Beghin, B., Hébert, J.-P., Steck, T., and Flaud, J.-M.: Monitoring tropospheric pollution using infrared spectroscopy from geostationary orbit, *C. R. Phys.*, 6, 888–896, 2005. 3494

Peuch, V.-H., Amodei, M., Barthet, T., Cathala, M.-L., Michou, M., and Simon, P.: MOCAGE, MOdèle de Chimie Atmosphérique à Grande Echelle, in: Proceedings of Météo France: Workshop on atmospheric modelling, Toulouse, FRANCE, 33–36, 1999. 3500, 3503

10 Peuch, V.-H., Attié, J.-L., Claeysman, M., Amraoui, L. E., Ricaud, P., Semane, N., Massart, S., Piacentini, A., Cariolle, D., Flaud, J.-M., Bergametti, G., Cantie, R., Pasternak, F., Lehors, L., von Clarmann, T., Höpfner, M., and Orphal, J.: Data assimilation experiments within the POGQA project, in: American Geophysical Union, Fall Meeting, San Francisco, California, USA, December, 2009. 3494

Peuch, V.-H., Orphal, J., and the MAGEAQ consortium: MAGEAQ: Monitoring the Atmosphere from Geostationary orbit for European Air Quality, Proposal submitted to ESA for Earth Explorer Opportunity Mission EE-8, 2010. 3494, 3501

Phillips, D.: A technique for the numerical solution of certain integral equations of first kind, *J. Ass. Comput. Mat.*, 9, 34–97, 1962. 3496

20 Pierangelo, C., Hébert, P., Rosak, A., Buil, C., and Bernard, F.: SIFTI, a Static infrared Fourier Transform Interferometer dedicated to ozone and CO pollution monitoring, in: International TOVS Study Conference (ITSC XVI), 5–13 May 2008, Angra dos Reis, Brasil, 2008. 3499

Pougatchev, N., August, T., Calbet, X., Hultberg, T., Oduleye, O., Schlssel, P., Stiller, B., Germain, K. St., and Bingham, G.: IASI temperature and water vapor retrievals – error assessment and validation, *Atmos. Chem. Phys.*, 9, 6453–6458, doi:10.5194/acp-9-6453-2009, 2009. 3502

Rodgers, C. D.: Inverse Methods for Atmospheric Sounding: Theory and Practice, Series on Atmospheric, Oceanic and Planetary Physics, Vol. 2, World Scientific, 2000. 3497, 3499

30 Rothman, L. S., Jacquemart, D., Barbe, A., Benner, D. C., Birk, M., Brown, L. R., Carleer, M. R., Chackerian, J. C., Chance, K., Coudert, L. H., Dana, V., Devi, V. M., Flaud, J.-M., Gamache, R. R., Goldman, A., Hartmann, J.-M., Jucks, K. W., Maki, A. G., Mandin, J.-Y., Massie, S. T., Orphal, J., Rinsland, A. P. C. P., Smith, M. A. H., Tennyson, J., Tolchenov, R. N.,

AMTD

3, 3489–3534, 2010

---

## Capabilities for a geostationary satellite to measure CO and O<sub>3</sub>

M. Claeysman et al.

---

Title Page

Abstract

Introduction

Conclusions

References

Tables

Figures

◀

▶

◀

▶

Back

Close

Full Screen / Esc

Printer-friendly Version

Interactive Discussion



**Capabilities for  
a geostationary  
satellite to measure  
CO and O<sub>3</sub>**

M. Claeysman et al.

Title Page

Abstract

Introduction

Conclusions

References

Tables

Figures

◀

▶

◀

▶

Back

Close

Full Screen / Esc

Printer-friendly Version

Interactive Discussion



Toth, R. A., Auwera, J. V., Varanasi, P., and Wagner, G.: The HITRAN 2004 molecular spectroscopic database, *J. Quant. Spectrosc. Ra.*, 96, 139–204, 2005. 3496

Rouil, L., Honoré, C., Vautard, R., Beekmann, M., Bessagnet, B., Malherbe, L., Meleux, F., Dufour, A., Elichegaray, C., FLaud, J.-M., Menut, L., Martin, D., Peuch, A., Peuch, V.-H., and Poisson, N.: An Operational Forecasting and Mapping System for Air Quality in Europe, *B. Am. Meteorol. Soc.*, 90(1), 73–83, 2008. 3504

Stillier, G. P., von Clarmann, T., Funke, B., Glatthor, N., Hase, F., Höpfner, M., and Linden, A.: Sensitivity of trace gas abundances retrievals from infrared limb emission spectra to simplifying approximations in radiative transfer modelling, *J. Quant. Spectrosc. Rad.*, 72 (3), 249–280, 2002. 3496

Stuhlmann, R., Rodriguez, A., Tjemkes, S., Grandell, J., Arriaga, A., Bézy, J.-L., Aminou, D., and Bensi, P.: Plans for EUMETSAT's Third Generation Meteosat (MTG) Geostationary Satellite Program, *Adv. Space Res.*, 36, 975–981, 2005. 3502

Tikhonov, A.: On the solution of incorrectly stated problems and a method of regularization, *Dokl. Acad. Nauk SSSR*, 151, 501–504, 1963. 3496

Turquety, S., Hadji-Lazaro, J., Clerbaux, C., Hauglustaine, D. A., Clough, S. A., Cassé, V., Schlüssel, P., and Mégie, G.: Operational trace gas retrieval algorithm for the Infrared Atmospheric Sounding Interferometer, *J. Geophys. Res.*, 109, D21301, doi:10.1029/2004JD004821, 2004. 3501

Turquety, S., Hurtmans, D., Hadji-Lazaro, J., Coheur, P.-F., Clerbaux, C., Josset, D., and Tsamalis, C.: Tracking the emission and transport of pollution from wildfires using the IASI CO retrievals: analysis of the summer 2007 Greek fires, *Atmos. Chem. Phys.*, 9, 4897–4913, doi:10.5194/acp-9-4897-2009, 2009. 3492

Vautard, R., Builtjes, P., Thunis, P., Cuvelier, K., Bedogni, M., Bessagnet, B., Honoré, C., Mousiopoulos, N., Schaap, M., Stern, R., Tarrason, L., and van Loon, M.: Evaluation and inter-comparison of Ozone and PM<sub>10</sub> simulations by several chemistry-transport models over 4 European cities within the City-Delta project, *Atmos. Environ.*, 41, 173–188, 2007. 3492

Worden, J., Liu, X., Bowman, K., Chance, K., Beer, R., Eldering, A., Gunson, M., and Worden, H.: Improved tropospheric ozone profile retrievals using OMI and TES radiances, *Geophys. Res. Lett.*, 34, L01809, doi:10.1029/2006GL027806, 2007. 3512

## Capabilities for a geostationary satellite to measure CO and O<sub>3</sub>

M. Claeysman et al.

**Table 1.** GEO-TIR and GEO-TIR2 instrument characteristics in the O<sub>3</sub> and CO thermal infrared band: Spectral Sampling Interval (SSI), Noise Equivalent Spectral Radiance (NESR) and Signal to Noise Ratio (SNR) calculated for a surface temperature of 280 K.

Sensor	Band	SSI (cm <sup>-1</sup> )	NESR (nW/(cm <sup>2</sup> sr cm <sup>-1</sup> ))	SNR
GEO-TIR	O <sub>3</sub>	0.05	6.04	750
GEO-TIR	CO	0.05	1.00	190
GEO-TIR2	O <sub>3</sub>	0.625	24.5	180
GEO-TIR2	CO	0.625	6.12	30

Title Page

Abstract

Introduction

Conclusions

References

Tables

Figures

◀

▶

◀

▶

Back

Close

Full Screen / Esc

Printer-friendly Version

Interactive Discussion



## Capabilities for a geostationary satellite to measure CO and O<sub>3</sub>

M. Claeys et al.

**Table 2.** Correlation (corr) bias and standard deviation (stdev) of the O<sub>3</sub> 0–3 km and 0–6 km columns (molecules/cm<sup>2</sup>) between MOCAGE model and GEO-TIR observations and between MOCAGE model and GEO-TIR2 observations for 6 European cities: Amsterdam, Berlin, London, Madrid, Paris and Rome. Positive bias indicate that observations are higher than MOCAGE and negative bias indicate than observations are lower than MOCAGE.

CITY	Column 0–3 km						Column 0–6 km					
	GEO-TIR – MOCAGE			GEO-TIR2 – MOCAGE			GEO-TIR – MOCAGE			GEO-TIR2 – MOCAGE		
	Corr	Bias %	Stdev %	Corr	Bias %	Stdev %	Corr	Bias %	Stdev %	Corr	Bias %	Stdev %
AMST.	0.81	10.3	16.8	–0.57	14.3	35.1	0.82	7.5	11.1	–0.54	10.0	27.3
BERLIN	0.81	6.5	12.7	–0.46	5.3	28.7	0.82	4.5	10.5	–0.42	2.9	25.0
LONDON	0.73	10.5	12.2	–0.37	17.8	22.8	0.78	8.6	8.7	–0.33	14.5	18.8
MADRID	0.73	0.8	12.9	0.30	–15.3	15.0	0.86	–1.5	6.9	0.47	–16.0	10.3
PARIS	0.71	7.8	11.3	–0.16	1.3	19.0	0.74	4.8	8.1	–0.14	–1.7	15.7
ROME	0.76	–11.4	9.4	0.52	–25.9	9.2	0.92	–7.9	6.2	0.66	–21.5	8.3

[Title Page](#)
[Abstract](#)
[Introduction](#)
[Conclusions](#)
[References](#)
[Tables](#)
[Figures](#)
[Back](#)
[Close](#)
[Full Screen / Esc](#)
[Printer-friendly Version](#)
[Interactive Discussion](#)


## Capabilities for a geostationary satellite to measure CO and O<sub>3</sub>

M. Claeysman et al.

**Table 3.** Same as Table 2 but for CO.

CITY	Column 0–3 km						Column 0–6 km					
	GEO-TIR – MOCAGE			GEO-TIR2 – MOCAGE			GEO-TIR – MOCAGE			GEO-TIR2 – MOCAGE		
	Corr	Bias %	Stdev %	Corr	Bias %	Stdev %	Corr	Bias %	Stdev %	Corr	Bias %	Stdev %
AMST.	0.83	–5.9	6.6	0.71	–10.6	7.9	0.89	–4.1	4.7	0.78	–8.1	6.1
BERLIN	0.83	–6.6	7.2	0.68	–11.5	9.0	0.89	–4.5	5.2	0.73	–8.7	7.5
LONDON	0.84	–6.1	6.2	0.64	–10.8	8.5	0.91	–4.1	3.9	0.76	–8.0	6.1
MADRID	0.79	–7.3	6.9	0.39	–8.4	10.5	0.86	–4.9	4.7	0.52	–5.0	8.1
PARIS	0.81	–13.9	9.7	0.66	–19.1	12.1	0.85	–9.6	7.3	0.72	–13.9	9.6
ROME	0.82	–11.6	9.7	0.74	–14.2	11.5	0.90	–6.0	6.0	0.85	–7.9	7.3

Title Page

Abstract

Introduction

Conclusions

References

Tables

Figures

⏪

⏩

◀

▶

Back

Close

Full Screen / Esc

Printer-friendly Version

Interactive Discussion



## Capabilities for a geostationary satellite to measure CO and O<sub>3</sub>

M. Claeysman et al.

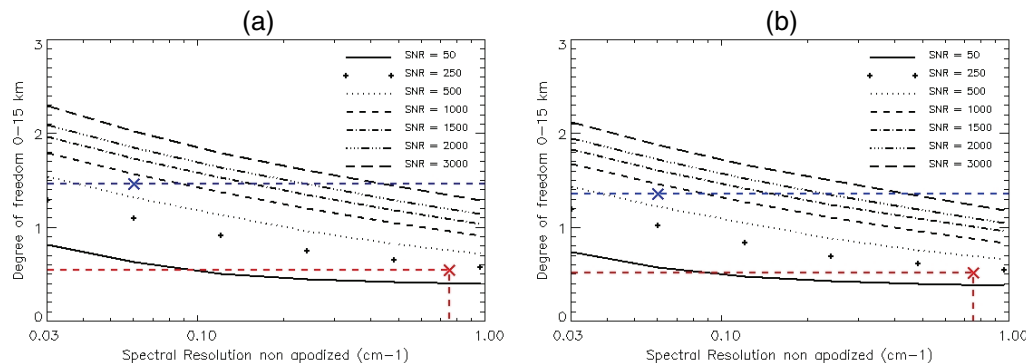


**Fig. 1.** Degrees of freedom (DOF) obtained for the O<sub>3</sub> retrieval as a function of spectral resolution (non apodized) and instrument noise (SNR): **(a)** positive thermal contrast (+2 K); **(b)** negative thermal contrast (−2 K). The DOFs have been obtained for an idealized case where all the parameters (e.g., regularization) are fixed except the SNR and the spectral resolution. The reference profile used to generate the synthetic measurement spectral radiances and representing the true profile in the retrieval study is an average of MOCAGE O<sub>3</sub> over Europe from 1 July 2009 to 31 August 2009 during daytime for the positive thermal contrast and during nighttime for the negative thermal contrast. The SNR is calculated for a surface temperature of 280 K. The blue cross corresponds to the GEO-TIR instrument configuration and the red cross corresponds to GEO-TIR2 instrument configuration.

[Title Page](#)
[Abstract](#)
[Introduction](#)
[Conclusions](#)
[References](#)
[Tables](#)
[Figures](#)
[◀](#)
[▶](#)
[◀](#)
[▶](#)
[Back](#)
[Close](#)
[Full Screen / Esc](#)
[Printer-friendly Version](#)
[Interactive Discussion](#)


## Capabilities for a geostationary satellite to measure CO and O<sub>3</sub>

M. Claeysman et al.

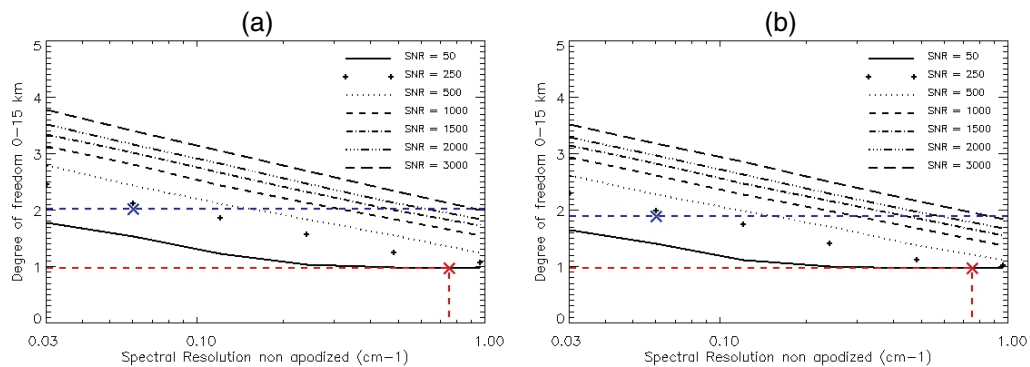


**Fig. 2.** Same as Fig. 1 but for CO.

Title Page

Abstract Introduction

Conclusions References

Tables Figures

⏪ ⏩

⏴ ⏵

Back Close

Full Screen / Esc

Printer-friendly Version

Interactive Discussion



## Capabilities for a geostationary satellite to measure CO and O<sub>3</sub>

M. Claeysman et al.

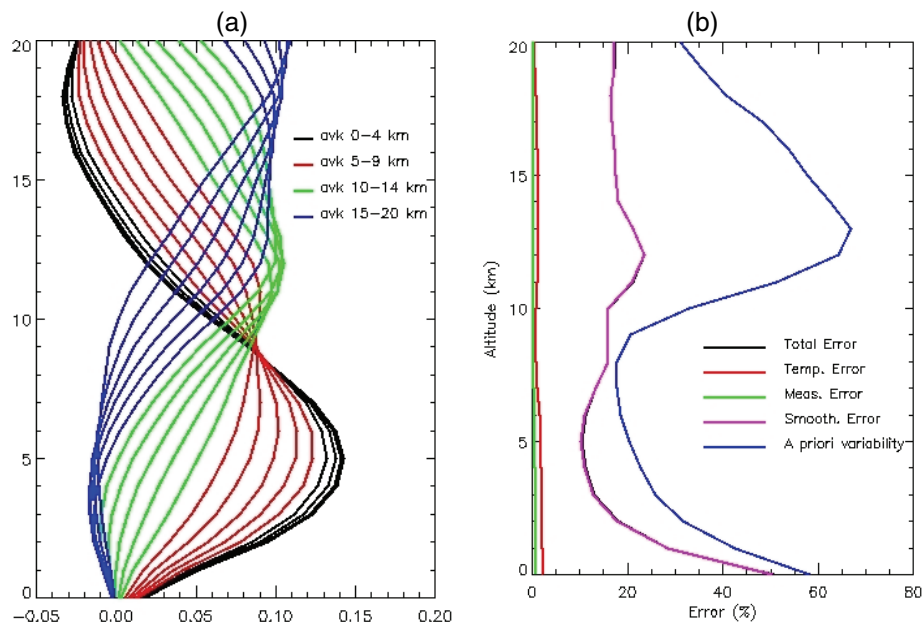


**Fig. 3.** (a) Averaging kernels obtained for the O<sub>3</sub> retrieval for a thermal contrast of 0 K: spectral sampling interval of 0.05 and a Signal to Noise Ratio (SNR) of 750 (0–4 km: black, 5–9 km: red, 10–14 km: green, 15–20 km blue); (b) error budget as a function of altitude for different error sources (see legend) for the same instrument characteristics as in part (a).

## Capabilities for a geostationary satellite to measure CO and O<sub>3</sub>

M. Claeys et al.

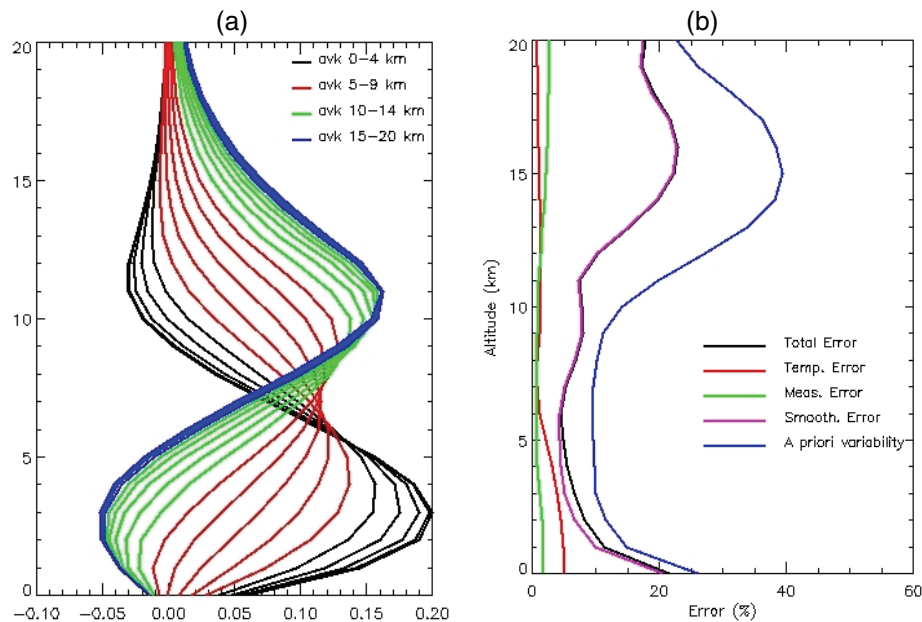


**Fig. 4.** Same as Fig. 3 but for CO.

[Title Page](#) | [Abstract](#) | [Introduction](#) | [Conclusions](#) | [References](#) | [Tables](#) | [Figures](#) | [Back](#) | [Close](#) | [Full Screen / Esc](#) | [Printer-friendly Version](#) | [Interactive Discussion](#)



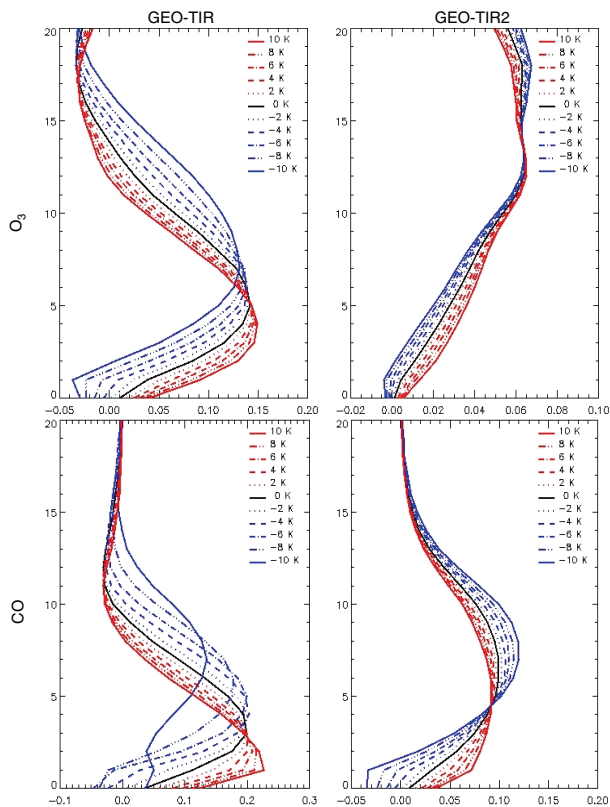


**Fig. 5.** First averaging kernel (surface level) calculated for different thermal contrasts from  $-10\text{K}$  to  $10\text{K}$  for GEO-TIR (left) and GEO-TIR2 (right) for  $\text{O}_3$  (top) and CO (bottom). Blue averaging kernels correspond to negative thermal contrast, red averaging kernels correspond to positive thermal contrast and the black averaging kernel correspond to a thermal contrast equal to 0 (see legend for line style).

**Capabilities for a geostationary satellite to measure CO and  $\text{O}_3$**

M. Claeysman et al.

Title Page

Abstract Introduction

Conclusions References

Tables Figures

⏪ ⏩

⏴ ⏵

Back Close

Full Screen / Esc

Printer-friendly Version

Interactive Discussion



## Capabilities for a geostationary satellite to measure CO and O<sub>3</sub>

M. Claeys et al.

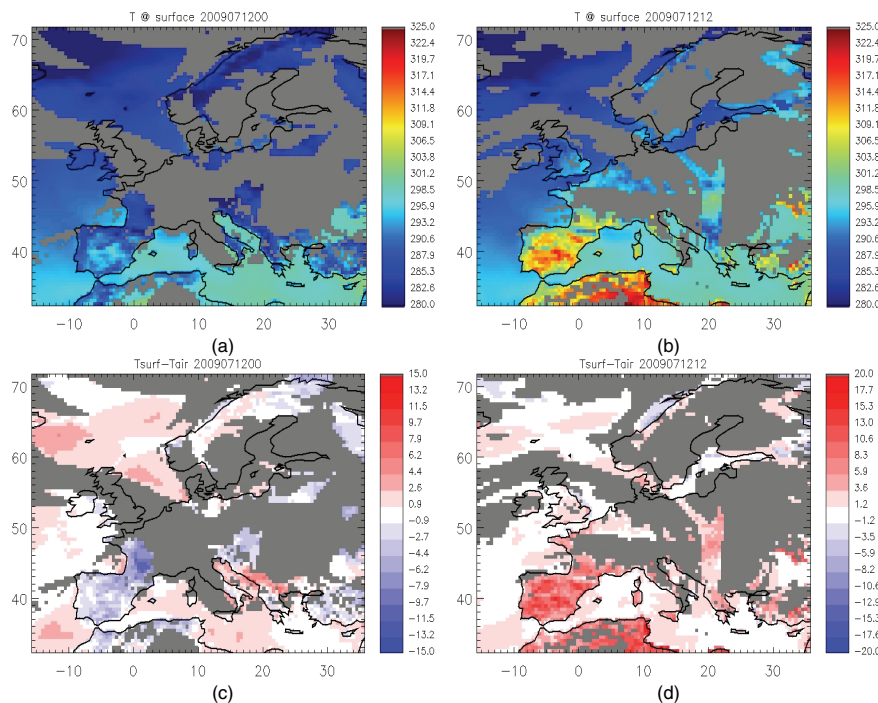


**Fig. 6.** Surface temperature in K (a, b) and thermal contrast (surface temperature minus air temperature near the surface) in K (c, d) on 12 July 2009 from ARPEGE: (left) 00:00 UTC; (right) 12:00 UTC. Grey areas represent pixels with more than 50% of cloud fraction. In (c, d) red indicates surface temperature is higher than the air temperature; blue indicates surface temperature is lower than the air temperature.

## Capabilities for a geostationary satellite to measure CO and O<sub>3</sub>

M. Claeysman et al.

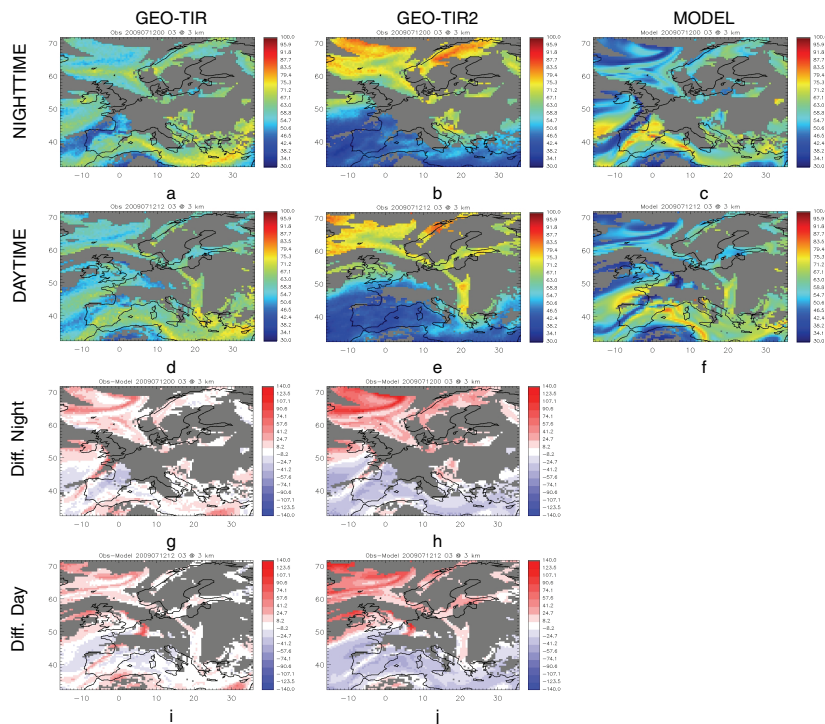


**Fig. 7.** O<sub>3</sub> fields in parts per billion by volume (ppbv) at 3 km on 12 July 2009 at 00:00 UTC (nighttime: top and third row) and at 12:00 UTC (daytime: second and bottom row) simulated by the MOCAGE model (**c**, **f**), and simulated by the Geostationary Observing System of GEO-TIR (**a** and **d**) and GEO-TIR2 (**b**, **e**) instruments. Relative difference (%) between simulated observations and model are shown for GEO-TIR (**g**, **i**) and for GEO-TIR2 (**h**, **j**) for nighttime (**g**, **h**) and daytime (**i**, **j**). Grey areas represent pixels with more than 50% of cloud fraction. In panels **g–j**, red indicates simulated observations are higher than the model results; blue indicates simulated observations are lower than the model results.

## Capabilities for a geostationary satellite to measure CO and O<sub>3</sub>

M. Claeysman et al.

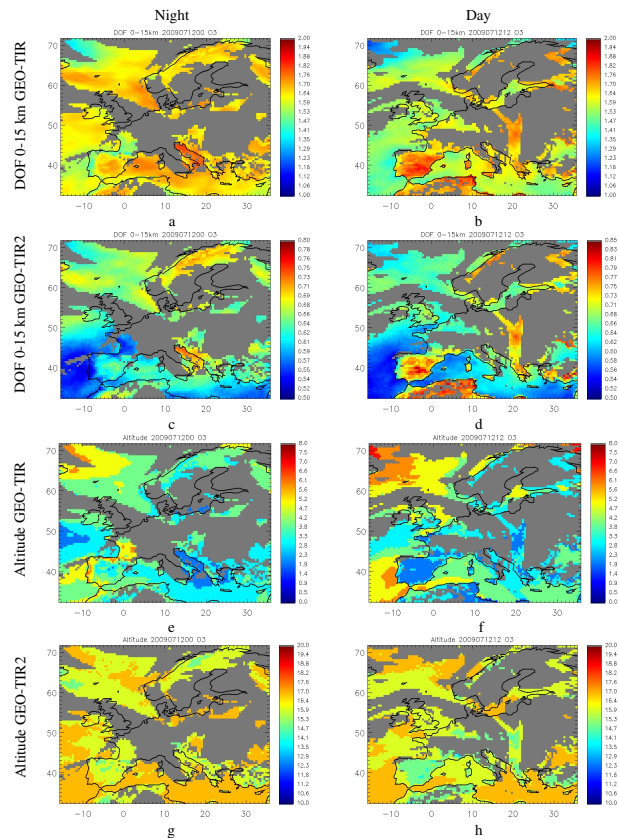


**Fig. 8.** Degrees of Freedom obtained for O<sub>3</sub> with GEO-TIR (**a**, **b**) and with GEO-TIR2 (**c**, **d**) instrument configuration on 12 July 2009 at 00:00 UTC (left) and at 12:00 UTC (right). The peak altitude (km) of the lowermost averaging kernels are represented for GEO-TIR (**e**, **f**) and for GEO-TIR2 (**g**, **h**) on 12 July 2009 at 00:00 UTC (left) and at 12:00 UTC (right). Grey areas represent pixels with more than 50% of cloud fraction. Note that the colour scales are different for GEO-TIR and GEO-TIR2.

[Title Page](#)
[Abstract](#)
[Introduction](#)
[Conclusions](#)
[References](#)
[Tables](#)
[Figures](#)
[Back](#)
[Close](#)
[Full Screen / Esc](#)
[Printer-friendly Version](#)
[Interactive Discussion](#)

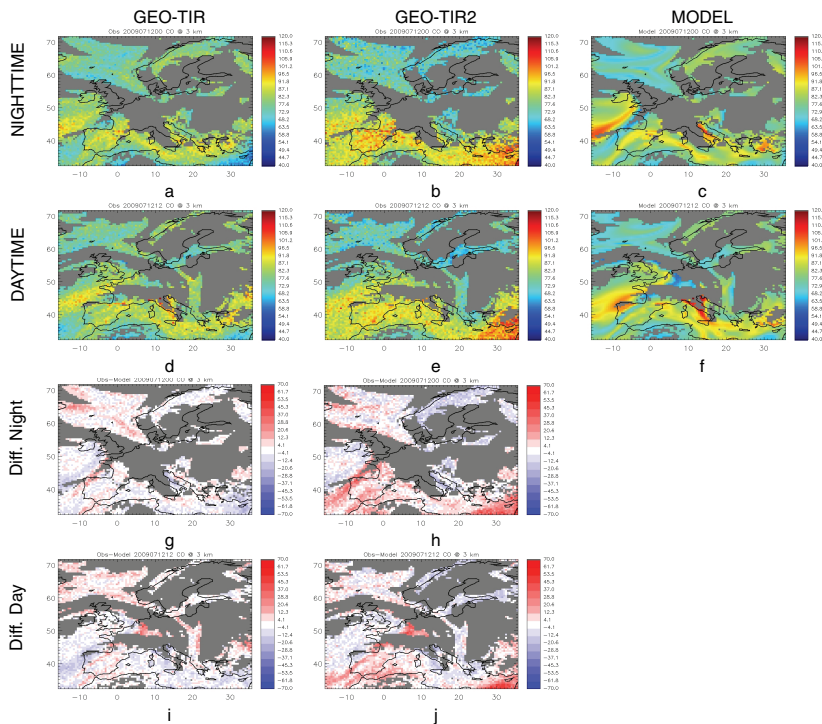


Fig. 9. Same as Fig. 7 but for CO.

## Capabilities for a geostationary satellite to measure CO and O<sub>3</sub>

M. Claeysman et al.

Title Page

Abstract

Introduction

Conclusions

References

Tables

Figures

◀

▶

◀

▶

Back

Close

Full Screen / Esc

Printer-friendly Version

Interactive Discussion

## Capabilities for a geostationary satellite to measure CO and O<sub>3</sub>

M. Claeys et al.

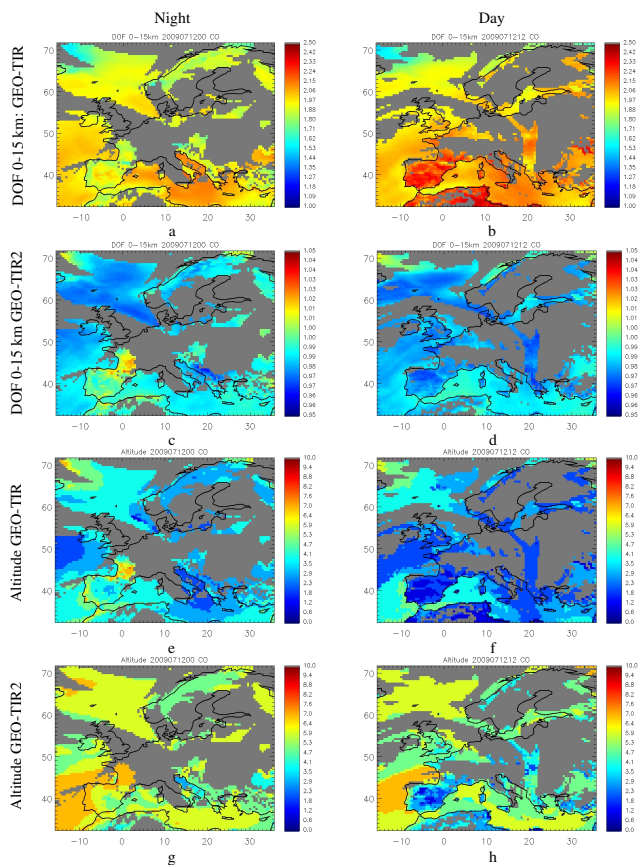


Fig. 10. Same as Fig. 8 but for CO.

Title Page

Abstract

Introduction

Conclusions

References

Tables

Figures

◀

▶

◀

▶

Back

Close

Full Screen / Esc

Printer-friendly Version

Interactive Discussion

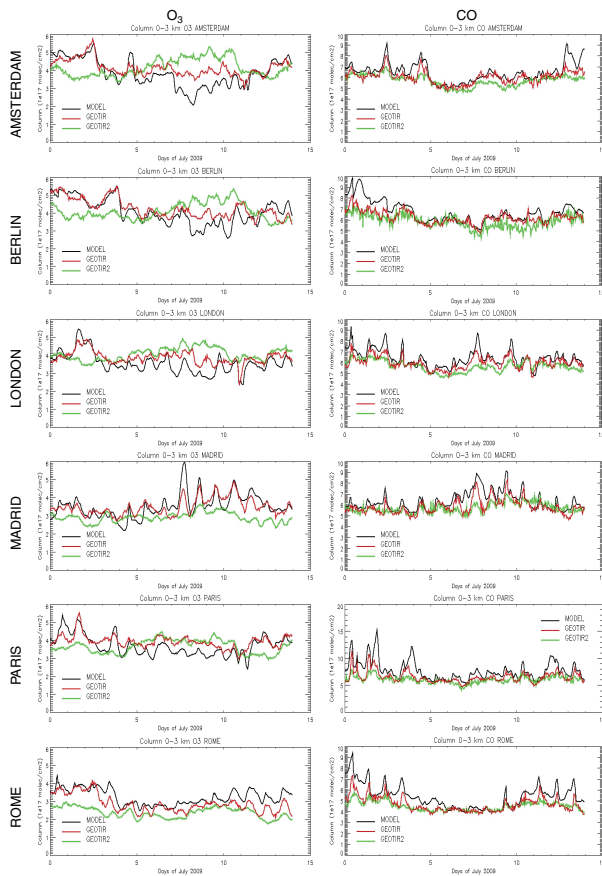


**Fig. 11.** Time-series of  $O_3$  (left) and  $CO$  (right) 0–3 km column (molecules/cm<sup>2</sup>) from 1–15 July 2009 with a temporal resolution of 1 h from the model MOCAGE (black line), GEO-TIR (red line) and GEO-TIR2 (green line) over 6 European cities, top to bottom panels: Amsterdam, Berlin, London, Madrid, Paris and Rome.

**Capabilities for a geostationary satellite to measure  $CO$  and  $O_3$**

M. Claeysman et al.

Title Page

Abstract Introduction

Conclusions References

Tables Figures

◀ ▶

◀ ▶

Back Close

Full Screen / Esc

Printer-friendly Version

Interactive Discussion

**Capabilities for  
a geostationary  
satellite to measure  
CO and O<sub>3</sub>**

M. Claeysman et al.

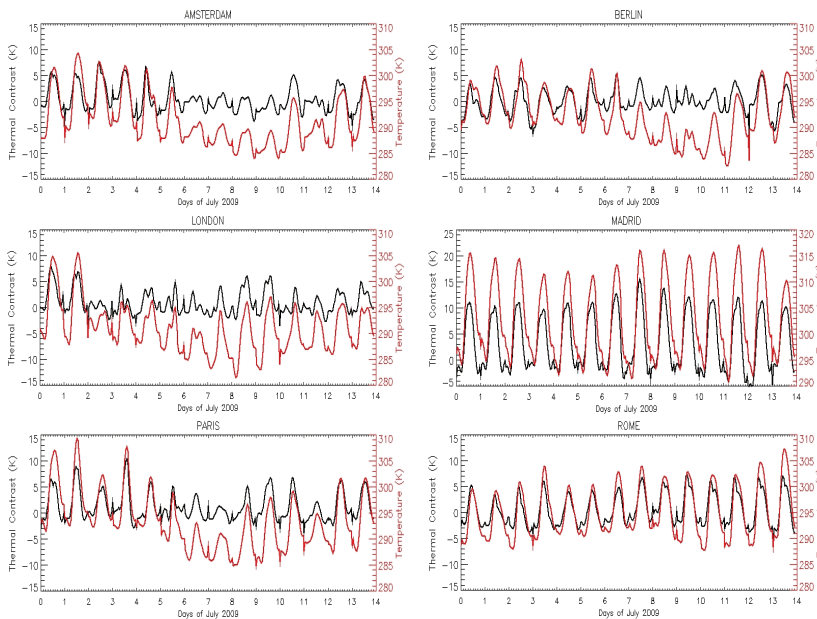


**Fig. 12.** Time-series of temperature at surface (red) and thermal contrast (black) in K from ARPEGE model from 1–15 July 2009 with a temporal resolution of 1 h over 6 European cities: Amsterdam, Berlin, London, Madrid, Paris and Rome.

[Title Page](#)[Abstract](#)[Introduction](#)[Conclusions](#)[References](#)[Tables](#)[Figures](#)[⏪](#)[⏩](#)[◀](#)[▶](#)[Back](#)[Close](#)[Full Screen / Esc](#)[Printer-friendly Version](#)[Interactive Discussion](#)